Available online at www.sciencedirect.com

ScienceDirect

Advances in Space Research 65 (2020) 2315–2323

ADVANCES IN SPACE RESEARCH (a COSPAR publication)

www.elsevier.com/locate/asr

Air-LUSI: A robotic telescope design for lunar spectral measurements

A. Cataford [a], S.A. Gadsden [a,*], K. Turpie [b]

[a] College of Engineering and Physical Sciences, University of Guelph, Guelph, ON N1G 2W1, Canada
[b] Joint Center for Earth Systems Technology, University of Maryland, Baltimore County, Baltimore, MD 21250, United States

Received 21 October 2019; received in revised form 1 February 2020; accepted 12 February 2020
Available online 23 February 2020

Abstract

This paper presents the mechanical design of a new robotic telescope that was designed and built to acquire lunar spectral measurements from the science pod of NASA's ER-2 aircraft while flying at an altitude of 70,000 feet (21.34 km). The robotic telescope used a double gimbal design that allowed for target tracking in azimuth and elevation. In addition to the challenging and restrictive geometry of the science pod, each component needed to be carefully selected to ensure that they could withstand the operating conditions at high altitude such as harsh temperatures extending as low as −54 °C and atmospheric pressure less than 1.05 psi (7.23 kPa). Due to the cold temperatures, low atmospheric pressure and the likely exposure to moisture, high strength industrial linear actuators were used to create an adjustable linkage system that controlled the pointing and tracking of the telescope. Although unconventional, this allowed for a robust design that outperformed the team's expectations by tracking the Moon for 40 min with an average tracking error under 0.05°. The results presented within this paper were acquired during a first set of engineering test flights, with further scientific missions to follow.

Keywords: Telescope; Earth observation; Robot; Design; Lunar measurement; NASA

1. Introduction

The air-born lunar spectral irradiance (air-LUSI) research project is a NASA-sponsored inter-agency project that is part of a long history to establish the Moon as a calibration source for Earth Observing Satellites. The ultimate goal is to establish a lunar calibration model that uses lunar phase and geometry to calibrate orbiting satellites using Earth bound LUnar Spectral Irradiance (LUSI) measurements (Cramer et al., 2013; Smith et al., 2012; Anderson et al., 1999; Cataford et al., 2019). Until recently, accurate Earth-bound LUSI measurements were impossible to acquire due to the atmospheric absorption of particular lunar wavelengths (Stone and Kieffer, 2006; Sun et al., 2008; Stone and Kieffer, 2002; Zimmer et al., 2010). To obtain highly accurate and unobstructed lunar spectral irradiance measurements, the air-LUSI project integrated instrumentation into NASA's ER-2 science aircraft and established the worlds first Airborne Lunar Observatory.

The air-LUSI project completed its first mission in 2018 over a two-night engineering test flight campaign and obtained the first unadulterated lunar spectral irradiance measurements from a semi ground-based system. The air-LUSI instrument was the product of three subsystem teams that are represented by the National Institute of Standards and Technology (NIST), the University of Guelph, and HAWK Institute for Space Sciences (Maryland). The NIST group was responsible for producing the IRradiance Instrument Subsystem (IRIS) to obtain radiometric measurements, while HAWK Institute for Space Sciences addressed all the heating requirements to extend the thermal limitations of sensitive equipment for high altitude conditions.

* Corresponding author.
E-mail address: gadsden@uoguelph.ca (S.A. Gadsden).

https://doi.org/10.1016/j.asr.2020.02.014
0273-1177/

The main contributions of this paper are to offer insight into the design challenges within the air-LUSI project, the robust equipment that was used to mitigate environmental risk, and mechanical considerations when implementing an air worthy pointing and tracking system for high altitude observations. This paper describes the design and construction of the novel Autonomous Robotic TElescope Mount Instrument Subsystem (ARTEMIS) that was capable of tracking the Moon from a moving aircraft at 70,000 feet (21.34 km). The paper also describes the constraints and considerations when designing an air-worthy robot that can operate in a confined space, with harsh environmental temperatures at −54 °C, low atmospheric pressure, and exposure to significant water condensation. The data acquisition and tracking accuracy during engineering flight tests is also summarized, followed by concluding remarks.

2. Design constraints

To obtain unobstructed lunar spectra, the robotic telescope observed the Moon through a windowless aperture of the science pod of the ER-2 aircraft and was therefore subjected to the harsh environmental conditions at high altitudes. Another concern was the limited areas of operation within the aft-pod and the attainable viewing angles provided by the window. Additionally, all structural and mechanical components used within the design needed to comply with the standards of the Airworthiness Review Committee at the NASA Armstrong Flight Research Center (AFRC). Given the requirements of the research project, the main design constraints pertained to the extreme environmental conditions, the structural and mechanical compliance with AFRC air worthiness standards, and the physical/viewing limitations of the aft-pod.

2.1. Environmental issues

For high altitude applications, the design must be able to withstand temperatures as low as −54 °C in addition to low atmospheric pressure. Not only does the low temperature exceed the operating range of most lubricants, but many lubricants are made with volatile chemicals that can vaporize at low atmospheric pressure. Additionally, as the aircraft descends from its high altitude to points of high humidity, extensive water condensation accumulates on anything that is open to the atmosphere. Therefore, special care needed to be taken to ensure that all electronics, actuators, and materials were adequately protected from moisture and that all materials were corrosion resistant.

2.2. Mechanical considerations

In addition to the environmental conditions, all equipment that is actively used within a NASA aircraft must pass review and inspection from the Airborne Sciences Flight Safety Review Committee of the AFRC. This implies that only aerospace-grade materials can be used in the construction of the instrument and material certifications must be preserved as supporting documentation. Also, all fasteners used within the design must meet Military Specifications (mil spec) and be accompanied by supporting documentation. An added constraint is that all fasteners must be installed with positive locking counterparts that meet mil spec standards. In addition to the design constraints, a detailed report outlining the minimum margins of safety for each component of the design must be submitted to AFRC engineers to prove the structural integrity of the design under crash landing conditions.

2.3. Geometric limitations

The AFRC team provided the dimensions of the aft section of the science pod. The design needed to fit within the void circular space of the internal structural rings of the aft pod which measured 29.80 in. (756.92 mm) in diameter. Fig. 1 is a model of the aft-section of the ER-2 science pod and shows the dorsal aperture through which the design viewed the Moon. AFRC also provided a standardized rack ('AFRC rack') that would contain the subsystem to facilitate the integration of the design to the aft-pod. The AFRC rack was a rectangle fabricated out of U channel aluminum that measured 33.50 in. (850.90 mm) in length, 24.75 in. (628.65 mm) in width, and provided an area of 5.76 sq-ft (0.54 m^2) to contain all structural and mechanical components of the air-LUSI robotic subsystem (ARTEMIS). Although the AFRC rack facilitated the integration of the instrument by sliding the system into the pod on horizontal rails that can be seen in Fig. 1b, it also limited the area of operation of the robotic telescope to the internal area of the rack. Table 1 provides a summary of all the dimensions limiting the area of operation of the design.

Another design challenge was to find an ideal mounting configuration for the telescope to optimize the available field-of-view when looking out of the viewport from inside the aft-pod. The range required by the design would target Moon elevations between 40° and 77° and provide an optimized azimuthal range to allow for mid-flight target tracking. The viewport of the aft-pod is a dorsal aperture having a narrow width of 8.00 in. (203.20 mm) and a chord length of 18.50 in. (469.90 mm) and provides only a vertical snapshot of the sky when looking straight up from inside the pod. These geometrical confines were further exacerbated when considering the size of the air-LUSI telescope which has a diameter of 6.125 in. (155.58 mm) and an overall length of 18.50 in. (469.90 mm).

3. Components of the robotic telescope

Given the environmental conditions that the design would be subjected to, extensive research went into finding rugged forms of actuation that offer wide operating temperatures, simple computer interfaces, and higher torque capabilities at a reasonable cost. In addition to methods of actuation, a large list of specialty bearings were

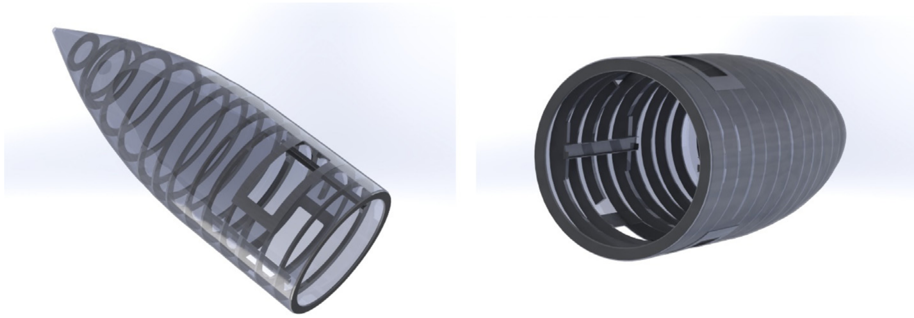

(a) Top view of pod. (b) Front view of pod.

Fig. 1. Rendering of NASA's ER-2 aft science pod.

Table 1
Geometric restrictions for the required design.

Restriction	Dimensions (in.)	Dimensions (m)
Pod Diameter	29.80	0.76
Telescope Length	18.10	0.46
Telescope Diameter	6.125	0.16
Pod Window	8.00	0.20
Chord Length	18.50	0.47
ARFC Rack	33.50 × 24.75	0.85 × 0.63

considered that offer minimal friction coefficients while providing free two degrees of rotational motion (Wang and Williams, 2008).

3.1. Ultra motion actuators

Given that the design only required a total displacement of approximately 45° in elevation and the azimuthal range was significantly restricted by the width of the aft-pod viewport, robust linear actuators were selected to control the telescope pointing. Using the linear actuators as a variable length linkage, the three-linkage system can be used to incite rotation of the telescope in both the azimuth and elevation.

Although linear actuators are a somewhat unconventional choice to control a double gimbal, using variable linkages to control angular position is fairly common when considering the use of hydraulics in heavy machinery. Furthermore, there are many examples of variable linkage systems using linear actuators to control pointing of telescopes, optical equipment, and solar panel heliostats (Cook et al., 2008; Saulescu et al., 2014). Additionally, by using the linear actuators as an alternative to conventional rotary motors, the mechanical design and manufacturing was significantly simplified by decreasing the number of mechanical components and lubrication points associated with gearing and bearings (Wang and Williams, 2008). An added benefit of the selected linear actuators was that they offered very fine position control and provided a high angular resolution while managing the pointing of the system (UltraMotion, 2018).

The design uses two Ultra Motion A2 series industrial linear actuators that interface to a control computer via RS-232 (UltraMotion, 2018). By using two independent controllers, position commands are written to each actuator to achieve desired pointing in elevation and azimuth. The full range of motion that is achievable using this configuration relies explicitly on the stroke length of each actuator, the distance between the pivot point of the telescope and the mounting point of the actuator, and the distance between the pivot point of the telescope and the connection point of the rod end of the actuator.

Aside from the benefits of a simplified mechanical design, the drawbacks associated with the use of linear actuators to control angular position is that the applied torque is non constant. In other words, the amount of force that is applied by the rod end of the linear actuator that is effective in producing a rotation is directly associated with the angle of attack between the linear actuator and the moving crank/linkage.

3.2. Kaman journal bearings

The careful review of many bearing and lubrication alternatives lead to the decision to use self lubricating journal bearings to obtain the low friction coefficients spanning temperature ranges of −54 °C to 40 °C. Among the many alternatives, the bearings that were used for the design were flanged journal bearings with a KAron VS liner offered by Kaman Speciality Bearings and Engineered Products (Kamatics, 2012, 2013). Although specialty ball bearings would have provided even smaller friction coefficients, their cost was significant when compared to the bushings.

The KAron VS bearings use a bonded liner as an alternative to polytetrafluoroethylene (PTFE) fabric-lined bearings. The KAron liner consists of a homogeneous mixture of resins, PTFE particles and other fillers (Kamatics, 2012). The bonding of the KAron liner to the bearing offers a uniform self-lubricating surface that is not susceptible to the same moisture concerns as PTFE mesh and fabric liners.

Among the many product options, the KAron VS journal bearings were selected based on their consistent low friction coefficients over a wide temperature range for moderate load conditions. The bearings can support up to a maximum dynamic pressure of 15,000 psi (103.42 MPa) and can operate between −73 °C and 150 °C. The liners also consist of very stable and inert materials that have very low moisture absorption characteristics which made them ideal for the environmental constraints of the air-LUSI robotic telescope design (Kamatics, 2012).

4. Robotic telescope design concepts

The most basic target tracking problem requires at a minimum a system with two degrees of freedom. To obtain this freedom of motion, a double gimbal consisting of two revolute joints is most commonly used to allow tracking of objects in azimuth and in elevation. These double gimbal systems can be seen in applications of defence, communications, and astronomy, and are commonly used to control the pointing and tracking of artillery, surveillance equipment, antennas, and telescopes.

To satisfy the freedom of motion of a double gimbal system all designs consist of shafts and bearings to provide smooth rotation of revolute joints, a strong base upon which the system can operate, actuators to adjust the pointing of the system, and trunnions to support the object that is being pointed. Aside from the common elements, there is a wide variation of gimbal alternatives that deviate in their sequencing of revolute joints and support structures and ultimately define the sight lines and range of motion available to the design (Osborne et al., 2008; Masten, 2008; Hurak and Rezac, 2009, 2012).

4.1. Bisecting axes design alternative

The first design alternative was created using a practical mechanical configuration. The design uses two bisecting axes to adjust the elevation of the telescope and allow for panning across the width of the window (Osborne et al., 2008; Cataford et al., 2018). The elevation axis consists of a trunnion table design that uses two journal bearings and two pivot points supported by the vertical and horizontal structural members shown in Fig. 2. The trunnion table offers an attached platform that would provide the mounting point of the actuator that adjusts the azimuth of the telescope.

The telescope assembly consists of a set of saddle clamps that are mounted on the circumference of the telescope cylinder and screw into concentric structural supports on the interior of the telescope tube. These saddle clamps are also connected together using flat plates that have small trunnion shafts protruding from the sides. This provides the azimuth pivot points and allows for the telescope assembly to be supported by a yoke.

The yoke is also coupled with the trunnion table and straddles the telescope about its second principle axis of rotation. Two bearings on either side of the yoke offer the second degree of freedom and allows the telescopes azimuth position to be adjusted using the second linear actuator (Osborne et al., 2008; Hilkert, 2008).

Although this design is mechanically convenient by grasping the telescope about its expected center of gravity and offering rotation about the telescope's primary inertial axes, the design is significantly disadvantaged when assessing the range of visibility when looking from the viewport of the aft-pod. The polar plot shown in Fig. 3 provides the azimuth and elevation angles when measured from the zenith that are achievable by the design. The concentric circular graduations provide the viewable elevation in degrees measured from the vertical while the graduations along the plot circumference provide the azimuthal range in degrees. The unobstructed view shown by the blue line was obtained by analyzing the available sight lines of the telescope using the geometry of the pod aperture, the telescope diameter, and the distances from the vantage point to the viewport edges.

By restricting the motion of the telescope to two bisecting axes, the vantage point of the telescope is limited to the intersection point of the two planes that contain the optical axis of the telescope and the elevation axis of the mount. With the 6.125 in. (155.58 mm) diameter telescope centred about the 8.00 in. (203.20 mm) pod aperture, the system would only have approximately 0.94 in. (23.88 mm) of play on either side to track a target in the azimuth.

Additionally, the elevation of the telescope is significantly limited by the horizontal extremities of the pod window that are separated by a chord length of 18.50 in. (469.90 mm). Given the size of the telescope, its limited

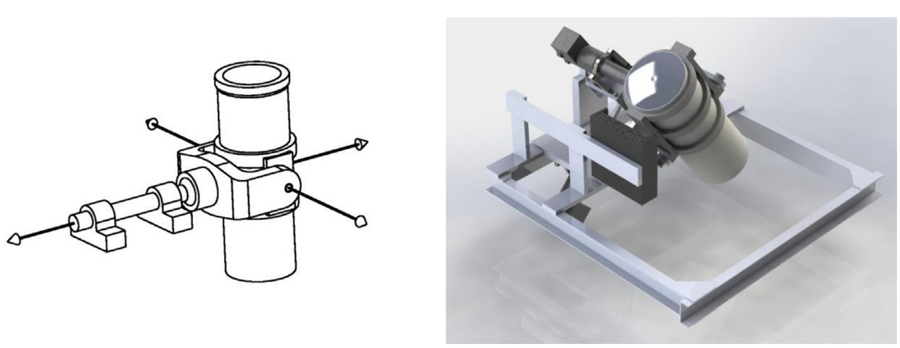

(a) Sketch showing two axes of rotation. (b) Rendering of the design.

Fig. 2. Mechanically balanced design of the robotic telescope used for lunar spectral measurements aboard NASA's ER-2 research aircraft.

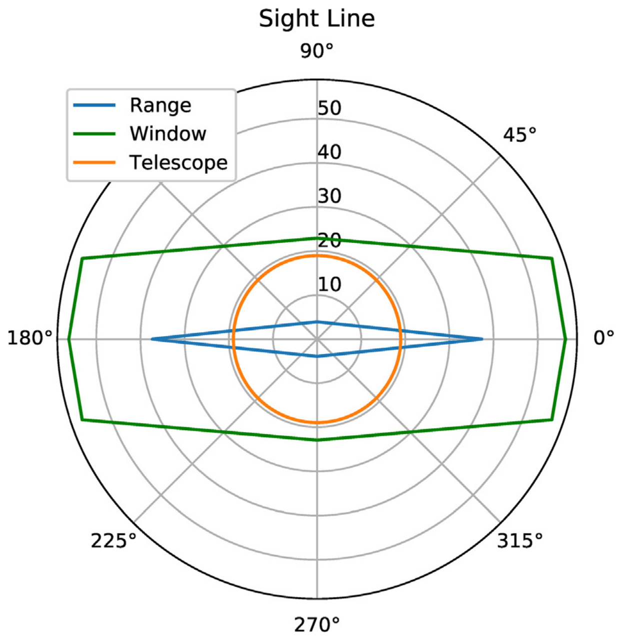

Fig. 3. Polar plot showing the telescope field of view with restrictions to window geometry and movement range of the telescope (mechanically balanced design).

attainable vantage points, and the restrictive geometry of the upward facing window, the design could only target Moon elevations of 63° measured from the horizontal with little to no tracking abilities over the width of the window.

Although this design had many mechanical benefits, it offered extremely limited lunar tracking abilities in elevation with a practically redundant azimuthal degree of freedom. Given the sightline analysis of the design, it became clear that to overcome the geometrical restrictions imposed by the aft-pod, the size of the telescope, and the upward facing window, a design would have to implement two offset axes that provided eccentric rotation of the telescope in both the azimuth and elevation.

4.2. Offset axes design alternative

Instead of the conventional telescope mounting of the first design, the following design shown in Fig. 4 uses two offset axes of rotation that do not correspond to the principal axes of inertia of the telescope. The telescope is still mounted using a trunnion configuration; however, the telescope assembly is supported by a trunnion base with an integrated linear actuator that adjusts its elevation. Given that the telescope trunnions are not coincident with one of the telescopes principle axes of inertia, the telescope is free to swing about its elevation axis. By mounting the telescope in this configuration, it expands the sight lines that can be used for tracking by physically displacing the vantage point of the telescope. The trunnion support is mounted on a vertically oriented shaft which allows for the entire telescope/trunnion subassembly to rotate and provide tracking in the azimuth.

Once again, the vertical shaft is offset from any principle axes of inertia of the telescope. Rather than having a fixed vantage point centred within the aft-pod viewport as seen in the first design, this alternative offers a sweeping vantage that can fall on any point of the arc that is created by the rotation of the telescope about its vertical and horizontal offset axes.

Given the increased area of operation achievable by this design, the sight lines are vastly increased and are more in line with the desired elevation ranges for lunar observations. Fig. 5 provides a polar plot showing the increased range of achievable elevations when measured from the zenith and the available range in azimuth. The polar plot provides a snap shot of the sky when looking out of the viewport from inside the aft-pod. The green and orange contours were added to provide context and outline the telescope and the aft-pod viewport. The area enclosed by the blue contour conveys the achievable azimuth and elevation angles of the telescope.

4.3. Selection of final design

The second design alternative was selected based on the increased Field of View that resulted from rotating the telescope about offset axes. All manufacturing of the design was completed at the University of Guelph using in house facilities. All structural components were manufactured out of Aluminum (6061-T6) to provide a strong design

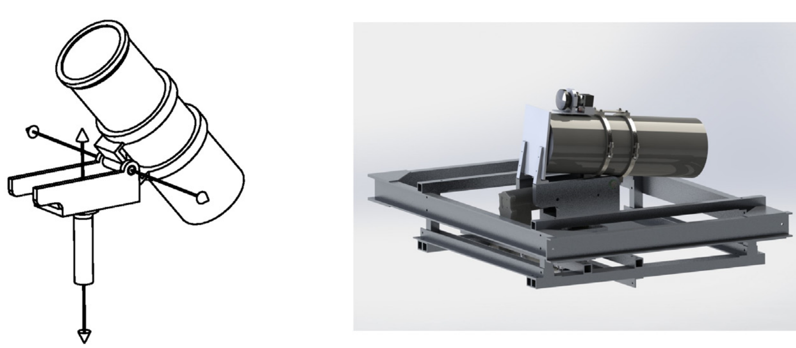

(a) Sketch showing two degrees of freedom. (b) Rendering of the design.

Fig. 4. Offset axes design alternative of the robotic telescope used for lunar spectral measurements aboard NASA's ER-2 research aircraft.

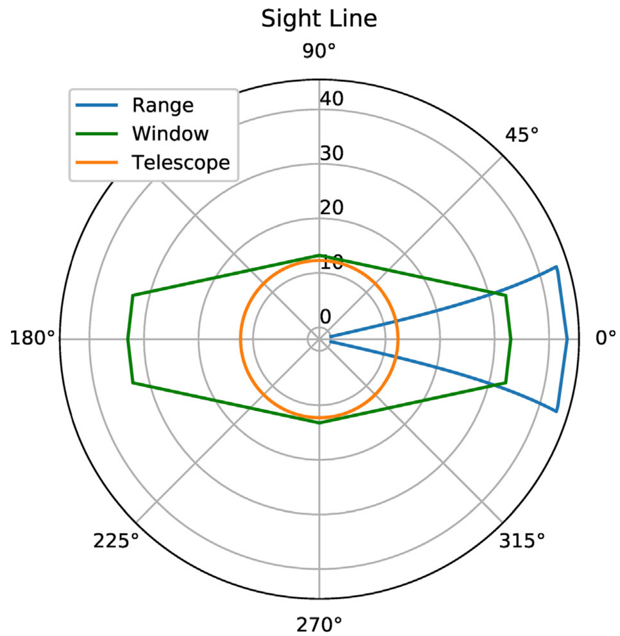

Fig. 5. Polar plot showing the telescope field of view with restrictions to window geometry and movement range of the telescope (offset axes design).

Table 2
Range of motion and pointing limits for the robotic telescope.

Limit	Elevation	Azimuth
Max	89°	15°
Min	46°	−15°

while decreasing its overall mass. The shafts and saddle clamps were machined out of stainless steel in an effort to increase the longevity of the design and decrease the maintenance associated with its components. Additionally, all fasteners used within the design were stainless steel Mil-Spec bolts and screws. All bolts used positive locking nuts to prevent loosening from vibration while all machine screws were threaded into locking HeliCoil inserts. The manufacturing process used only aerospace grade materials and the design was deemed Flight Worthy and met the standards of the Flight Safety Review committee at AFRC.

The achievable sight lines of the constructed design are provided in Table 2 and present the maximum and minimum pointing angles in elevation (measured from the horizontal) and azimuth. Note that the range of motion was larger than the line of sight due to the ER-2 window openings and fuselage, which would cause clipping of the telescope view.

5. Data acquisition

Aside from the mechanical aspects of the design, the robotic telescope mount used a machine vision camera to acquire target and tracking data. Additionally, an Inertial Measurement Unit (IMU) was attached to the telescope to acquire validating data for post flight analysis. Overall, the performance of the design during its first flight campaign was completed based on the targeting data acquired from the tracking camera, the position data from the elevation and azimuth actuators, and the trends observed in the IMU data.

The following sections provide some performance validating plots. The data was collected during the first air-LUSI engineering flight campaign that occurred on August 2nd 2018. The data represents the tracking performance of the design over a 40-minute timeframe while the ER-2 aircraft flew at an altitude of 70,000 feet.

5.1. Camera and IMU subassembly

The autonomous tracking system of the design relied on a machine vision camera that was mounted near the aperture of the telescope. By processing the incoming frames of the tracking camera, the x and y pixel location of the target was obtained (Hurak and Rezac, 2009, 2012; Park et al., 2011; Bonadies et al., 2017; Cataford et al., 2018; Baek et al., 2016). Using this data, the error between the pixel position of the target and a desired pixel position was used as inputs to two PID controllers (Gadsden, 2017). The two controllers then provided a calculated control effort that was sent to the linear actuators and forced the error between the target and the setpoint to converge to zero.

The tracking camera was a Basler (acA1920-40um) which is a 2.3-megapixel monochromatic camera that can operate at 42 fps. The wide-angle lens provided a large snapshot of the sky and was therefore capable of viewing targets anywhere within the sight lines of the aft-pod viewport.

Fig. 6a shows the tracking camera and lens with accompanying supports in addition to the integrated rugged VN-100 IMU. The camera lens is fixed in position using a bored-out base with an accompanying saddle clamp. This allowed the lens to be supported in position while resisting any moments acting on it when attached to the camera. A small aluminum block was machined to provide a camera mounting platform that ensured that the optical axes of the camera and the lens were aligned.

A recessed section of the camera base was created to provide space for an integrated Inertial Measurement Unit (IMU) as seen in Fig. 6b. The IMU was integrated with the camera assembly to obtain validating measurements of the design when operating autonomously from the aircraft.

5.2. Actuator movements

The following plots depict the azimuth and elevation actuator positions during the tracking phase of the mission. The linear actuators consist of a servo motor that rotates a lead screw and produces a linear displacement of the lead screw nut. The displacement of the nut provides the linear motion of the actuator shaft which pivots the telescope about its elevation and azimuth axes. A phase index

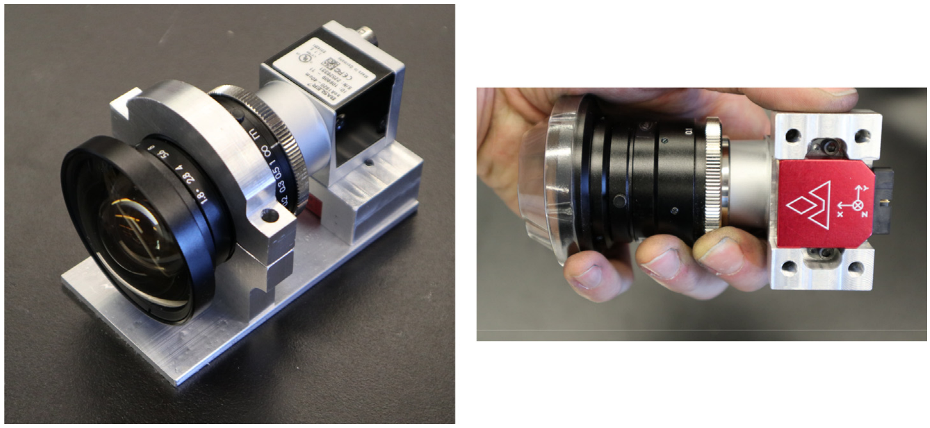

(a) Basler tracking camera. (b) View of the integrated IMU.

Fig. 6. Camera IMU subassembly used to track the Moon.

position sensor provides actuator position data and is also used by the linear actuators internal computer/control system (UltraMotion, 2018).

Fig. 7a provides the phase index sensor values that are used to interpret the linear actuator positions. The positions (mapped as actuator encoders or 'enc') are plotted against the UTC time stamps to present a time series of the actuator data. Each graduation of the time series is separated into 5-minute blocks. The azimuth actuator position shows that the system locks on to the azimuth position of the Moon which corresponds to approximately 19,200 integer position units. This azimuthal position remains relatively constant for the 40-minute tracking phase, with the exception of the ±500 position unit corrections resulting from flight disturbances to the system.

Much of the same traits are observed in Fig. 7b with one interesting difference. By inferring a trend line of the data, we can actually observe the steady decrease in lunar elevation over the 40-minute tracking window. At the beginning of the tracking phase, the elevation actuator locks onto the Moon with a position of approximately 15,350. After 40 min of tracking, the lunar elevation decreased to an associated actuator position of approximately 14,500. During that time, the control system introduced small incremental changes of approximately ±250 position units to compensate for the system disturbances resulting from the relative motion of the aircraft.

5.3. Tracking accuracy

The best metric to assess the tracking performance of the design was the pixel error in (x,y) between the center of the Moon and the pixel setpoint. The pixel setpoint was determined prior to the flight campaign by aligning the telescope with a distant light source, determining its location within the tracking camera frames, and calculating a parallax correction for the pixel setpoint. This resulted in a desired pixel position that would center a target within the field of view of the telescope.

The pixel error plots in X and Y shown by Fig. 8 provide a basis to evaluate the tracking performance of the azimuth and elevation controllers, while Fig. 9 represents the total tracking error which can be interpreted as the radial distance separating the Moon center from the established

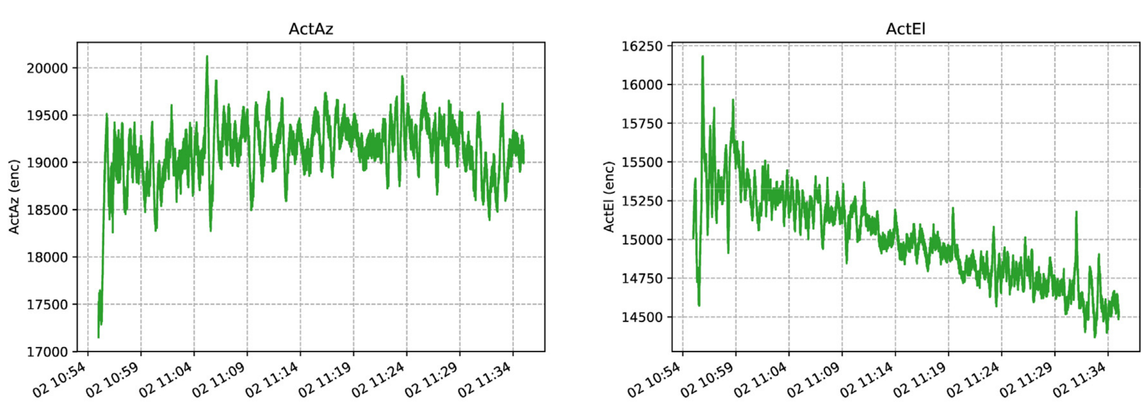

(a) Azimuth actuator position during flight. (b) Elevation actuator position during flight.

Fig. 7. ARTEMIS actuator positions during lunar spectral collection.

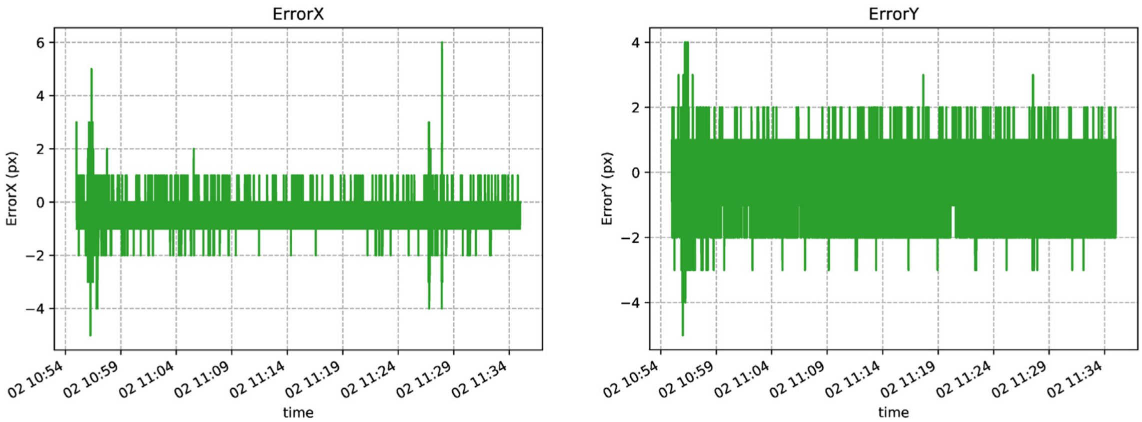

(a) Pixel error in the x-axis.

(b) Pixel error in the y-axis.

Fig. 8. Camera tracking pixel errors during lunar collection.

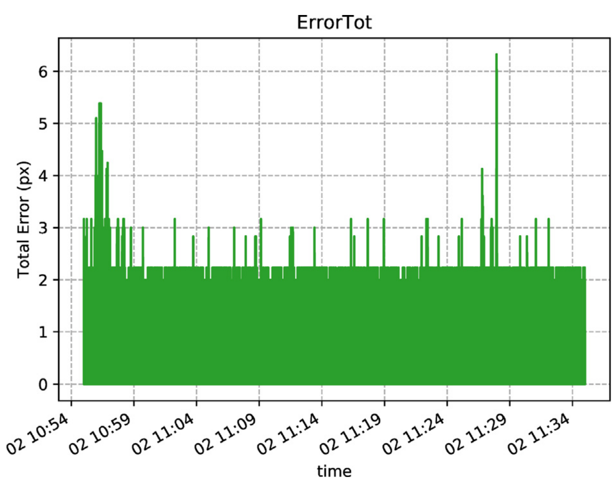

Fig. 9. Sample of total pixel error during engineering flights.

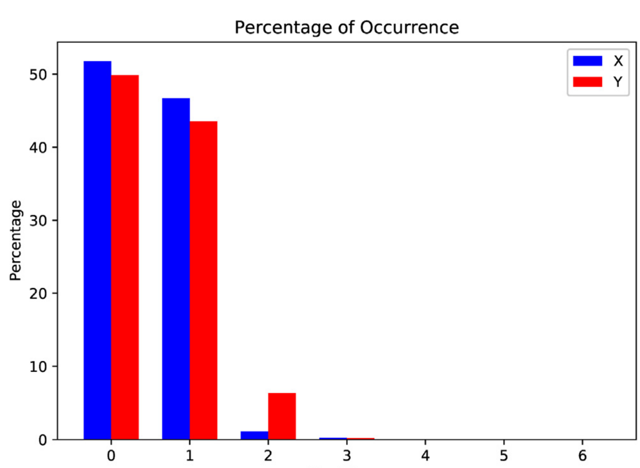

Fig. 10. Percentage of pixel error occurrences.

pixel setpoint. The pixel values in (x,y) only take on integer values and therefore, the two plots shown in Fig. 8 consist of a 40 min time series of discrete integer steps. Based on the tracking statistics, it appears that the elevation controller performed slightly better than azimuth controller by keeping the Moon within $-5 \leq \theta_{el} \leq 4$ and $-5 \leq \theta_{az} \leq 6$ pixels of the respective setpoints (see Fig. 10.).

The radial offset of the Moon center from the setpoint is obtained by adding the coinciding x and y errors in quadrature. Given the lens and camera combination, a single pixel corresponds to an angular offset of 0.053°. The design achieved an average total tracking error of 0.91 pixels which corresponds to 0.048°. Of course this does not suggest that the system maintained this level of performance through out the entire tracking phase of the mission; however, it does provide a good metric to condense the performance of the design to a single value. Table 3 offers a summary of the tracking statics based on the x, y, and total pixel offsets from the setpoint.

The following histogram shows the percentage of occurrences of pixel error throughout the 40-minute tracking window for x and y. Although this plot does not imply that the pixel error occurrences in x and y coincide with the same time stamp, it does provide a compelling visual reference to convey the performance of the tracking system. Among the total number of data points collected during the tracking portion of the mission, approximately 50% of the tracking error data points were 0 pixels from the setpoint, while 46% of the tracking errors were at a 1 pixel offset. This suggests that the center of the Moon was within ±1 pixel of the setpoint for 96% of the collected data.

Table 3
Tracking statistics for pixel error during engineering flights.

Statistic	X	Y	Radial Offset	Degree Offset
Mean	−0.43	0.32	0.91	0.048°
STD	0.61	0.78	0.66	0.035°
Min Value	−5.00	−5.00	0.00	0.000°
Max Value	6.00	4.00	6.32	0.335°
RMSE	0.74	0.84	1.12	0.059°
Median	0.00	0.00	1.00	0.053°
Mode	0.00	0.00	(0.00 & 1.00)	(0.000° & 0.053°)

6. Conclusions

The air-LUSI design of a robotic telescope proved to be very effective based on the results obtained from its first airborne deployment in August 2018. The primary challenges for the project were to produce a mechanical design that could be seamlessly integrated into the science pod of the ER-2 and that yielded sight lines ranging from 44° to 77° from the viewport. The novelty of the airborne robotic telescope design was the use of high-resolution linear actuators to adjust the pointing of the telescope and a machine vision camera to target the Moon while in flight. The adjustable linkage system provided fine pointing accuracy in azimuth and elevation angles while providing actuators that were extremely resilient to the harsh operating environments. The success of the first set of engineering flights validated the mechanical design, allowing the system to obtain the first set of lunar spectral irradiance measurements with the control system keeping the Moon within an averaged tracking error of 0.05° of the setpoint (an order of magnitude better than required). Given the performance of the system, further software development is ongoing and additional functionality is currently being added in preparation for future flight campaigns.

Acknowledgements

We would like to recognize the efforts of Steven Brown, Steven Grantham, John Woodward, and Stephen Maxwell at the National Institute of Standards and Technology (NIST, Gaithersburg, Maryland). Their telescope design, collaboration, and optical expertise were essential to the success of this research project.

This work was partially funded under the NASA Airborne Instrument Technology Transfer Program via Grant NNX17AL25G titled "Development of a Highly Accurate Lunar Spectral Irradiance Measurement Capability – The Airborne LUnar Spectral Irradiance Instrument (air-LUSI)," as well as by the Natural Sciences and Engineering Research Council of Canada and the University of Guelph.

References

Anderson, J., Becker, K., Kieffer, H., Dodd, D.N., 1999. Real-time control of the robotic lunar observatory telescope. Publ. Astron. Soc. Pac. 111 (760), 737–749.

Baek, I. et al., 2016. Whole-surface round object imaging method using line-scan hyperspectral imaging system. Baltimore, Maryland, SPIE Sensing for Agriculture and Food Quality and Safety VIII.

Bonadies, S. et al., 2017. An overview of autonomous crop row navigation strategies for unmanned ground vehicles. ASME J. Dyn. Syst. Meas. Control 140 (6), 1–6.

Cataford, A., Gadsden, S.A., Turpie, K., 2019. Air-lusi: Autonomous telescope design for lunar spectral irradiance measurements. SPIE Advanced Optics for Imaging Applications, UV through LWIR IV, Baltimore, Maryland.

Cataford, A., Gadsden, S. A., Turpie, K. & Biglarbegian, M., 2018. Air-LUSI: Estimation, filtering, and PID tracking simulation. In: Quebec City, Quebec, IEEE Canadian Conference on Electrical and Computer Engineering (CCECE).

Cook, B. et al., 2008. Precision linear actuator for space interferometry mission (sim) siderostat pointing. In: Huntsville, Alabama, 39th Aerospace Mechanisms Symposium.

Cramer, C.E., Lykke, K.R., Woodward, J.T., Smith, A.W., 2013. Precise measurement of lunar spectral irradiance at visible wavelengths. J. Res. Nat. Inst. Stand. Technol. 117 (1), 737–749.

Gadsden, S.A., 2017. An adaptive PID controller based on bayesian theory. In: Tysons Corner, Virginia, ASME Dynamic Systems and Control Conference.

Hilkert, J., 2008. Inertially stabilized platform technology. IEEE Control Syst. Mag. 28 (1), 26–46.

Hurak, Z., Rezac, M., 2009. Combined line-of-sight inertial stabilization and visual tracking: application to an airborne camera platform. In: Shanghai, China, 48th IEEE Conference on Decision and Control and 28th Chinese Control Conference.

Hurak, Z., Rezac, M., 2012. Image-based pointing and tracking for inertially stabilized airborne camera platform. IEEE Trans. Control Syst. Technol. 20 (5), 1146–1159.

Kamatics, 2012. KAron Design Guide. Specialty Bearings and Engineered Products, Bloomfield, Conneticut.

Kamatics, 2013. KAron Bearing Catalog: Spherical, Rod End, and Journal Sleeve Bearings. Specialty Bearings and Engineered Products, Bloomfield, Conneticut.

Masten, M., 2008. Inertially stabilized platforms for optical imaging systems. IEEE Control Syst. Mag. 28 (1), 47–64.

Osborne, J., Hicks, G., Fuentes, R., 2008. Global analysis of the double-gimbal mechanism. IEEE Control Syst. Mag. 28 (4), 44–64.

Park, J. et al., 2011. A novel method for vision tracking with line of sight control, using a fuzzy logic controller and Euler angle orientation in the feedforward loop. In: Incheon, South Korea, 8th International Conference on Ubiquitous Robots and Ambient Intelligence (URAI).

Saulescu, R., Munteanu, O., Neagoe, M., Cretescu, N., 2014. On the eccentricity effects in solar tracking triangular linkage with eccentric linear actuator. Mech. Mach. Sci. 17 (1), 209–216.

Smith, A., Lorentz, S., Stone, T., Datla, R., 2012. Lunar spectral irradiance and radiance (lusi): New instrumentation to characterize the moon as a space-based radiometric standard. J. Res. Nat. Inst. Stand. Technol. 117 (1), 185–201.

Stone, T., Kieffer, H., 2002. Absolute Irradiance of the Moon for On-orbit Calibration. SPIE Earth Observing Systems VII, San Diego, California.

Stone, T., Kieffer, H., 2006. Use of the Moon to Support On-orbit Sensor Calibration for Climate Change Measurements. SPIE Earth Observing Systems XI, San Diego,California.

Sun, J. et al., 2008. MODIS and SeaWIFS On-orbit Lunar Calibration. SPIE Earth Observing Systems XIII, San Diego, California.

UltraMotion, 2018. Servo Cylinder Information and User Manual Version. Ultra Motion, Cutchogue, New York.

Wang, H., Williams, T., 2008. Strategic inertial navigation systems. IEEE Control Syst. Mag. 28 (1), 65–85.

Zimmer, P. et al., 2010. Space-based Photometric Precision from Ground-based Telescopes. SPIE Fround-based and Airborne Instrumentation for Astronomy III, San Diego, California.